

## Back-Face Strain Compliance and Electrical-Potential Crack Length Calibrations for the Disk-Shaped Compact-Tension DC(T) Specimen

Authorized Reprint 1994 from Journal of Testing and Evaluation, March 1994  
Copyright American Society for Testing and Materials, 1916 Race Street, Philadelphia, PA 19103

**REFERENCE:** Gilbert, C. J., McNaney, J. M., Dauskardt, R. H., and Ritchie, R. O., "Back-Face Strain Compliance and Electrical-Potential Crack Length Calibrations for the Disk-Shaped Compact-Tension DC(T) Specimen," *Journal of Testing and Evaluation*, JTEVA, Vol. 22, No. 2, March 1994, pp. 117-120.

**ABSTRACT:** Back-face strain compliance and electrical-potential crack length calibrations have been experimentally determined for the disk-shaped compact-tension DC(T) specimen. Finite-element modeling was used to ascertain the back-face strain distribution at several crack lengths to determine the significance of inconsistent gage placement. The numerical solutions demonstrated good agreement with experiment, especially at smaller crack lengths when the back-face strain gradients are minimal. It is concluded that precise gage placement is only critical when the crack tip closely approaches the back of the test specimen.

**KEYWORDS:** back-face strain compliance, electrical-potential calibration, disk-shaped compact-tension DC(T) specimen

The disk-shaped compact-tension DC(T) specimen (Fig. 1), as defined in ASTM E 399, Test Method for Plane-Strain Fracture Toughness of Metallic Materials, has recently been the focus of increased use in the field of fracture and fatigue of advanced materials, specifically for resistance-curve and crack-growth measurements in monolithic and composite ceramics and intermetallics (e.g., Refs 1 through 3). The geometry is appealing due to the limited availability of these materials and the methods by which they can be processed; procedures often involve the hot-pressing of powders into cylindrical rod form, which then can be readily sliced into a large number of DC(T) specimens.

The Mode I linear-elastic stress-intensity ( $K_I$ ) solution for this geometry is well known [4], viz.

$$K_I = \frac{P}{BW^{1/2}} f(a/W),$$

$$f(a/W) = \frac{2 + a/W}{(1 - a/W)^{3/2}} [0.76 + 4.8(a/W) - 11.58(a/W)^2 + 11.43(a/W)^3 - 4.08(a/W)^4] \quad (1)$$

Manuscript received 7/20/93; accepted for publication 10/11/93.

<sup>1</sup>Center for Advanced Materials, Materials Sciences Division, Lawrence Berkeley Laboratory and Department of Materials Science and Mineral Engineering, University of California, Berkeley, CA 94720.

where  $P$  is the applied load, and  $a$ ,  $B$ , and  $W$  are, respectively, the crack length, thickness, and width of the specimen; Eq 1 is accurate to within  $\pm 0.3\%$  for  $0.2 \leq a/W \leq 1$ . However, calibrations for electrical-potential crack-length monitoring and back-face strain compliance are not presently tabulated in the literature for this geometry. These relationships are useful for the *in situ* measurement of subcritical crack-growth rates (see ASTM E 647, Test Method for Measurement of Fatigue Crack Growth Rates). Back-face strain compliance has also been useful as a technique to monitor crack length during high-temperature fracture and fatigue testing where clip gages are impractical [5]. In addition, back-face strain can be used to assess the extent of fatigue crack closure [6] as well as the magnitude of crack-bridging effects in the wake of the crack tip [7]. As such crack-tip shielding by closure and bridging phenomena are known to have a significant effect on the toughening and cyclic fatigue degradation of most ceramics and intermetallics of technological interest (e.g., Refs 8 through 10), the objective of the study was to determine these calibrations for this specimen geometry.

### Experimental Procedures

Two DC(T) specimens were machined from AISI 304 stainless steel to the dimensions indicated in Fig. 1. To measure compliance, a 350  $\Omega$  strain gage with a 1.57 mm gage length was attached to the back face of each specimen, centered along a diameter commensurate with the machined notch (Fig. 2). To provide a standard measure of crack length, a 10 mm NiCr Krak<sup>®2</sup> gage was attached to one side surface; the resolution of this gage was  $\pm 2 \mu\text{m}$ . In addition, fracture surfaces were periodically marked (see below) to provide a check on the Krak gage readings.

Cracks were grown by cyclic fatigue at a constant applied stress-intensity range of  $\Delta K = 20 \text{ MPa}\sqrt{\text{m}}$  with a load ratio  $P_{\text{min}}/P_{\text{max}}$  of 0.3. The load ratio was selected such that crack-closure effects (which result in a deviation from linearity in the load versus back-face strain curve) were not observed. Approximately every 0.10 mm of crack extension, measurements of elastic compliance ( $C = \delta/P$ , where  $\delta$  is the back-face strain) were taken during unloading. Similarly, measurements of the electrical-potential difference  $V$  between two points 1 mm above and

<sup>2</sup>Hartrun Corp., TTI Division, St. Augustine, FL.

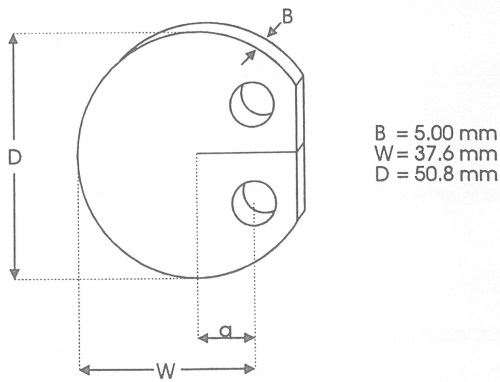


FIG. 1—The standard disk-shaped compact-tension DC(T) specimen, as defined in ASTM E 399.

below the notch were taken (Fig. 2); a direct current of roughly 35 A was applied to the specimen such that the initial voltage  $V_0$  across the starter notch (with  $a_0/W = 0.30$ ) was 5 mV. Procedures and precautions for the electrical-potential calibration conform to those outlined in the Metals Handbook [11]. The placement of the potential measurement probes was chosen for optimum sensitivity and reproducibility, as described in Ref 12 for the C(T) specimen. In order to supply sufficient room to anchor securely the current lead connections, however, these were placed as indicated in Fig. 2. To allow for possible crack-bowing effects, specimens were overloaded (by ~80% over the baseline stress-intensity level) every ~1 mm of crack extension to mark the fracture surface; this permitted measurement of the mean through-thickness crack length and provided an additional check of the Krak gauge readings of crack length.

### Numerical Methods

Finite-element modeling (FEM) was performed to ascertain the back-face strain distribution at three different values of  $a/W$  (0.30, 0.53, and 0.80) in order to determine the sensitivity to gage placement along the back surface and to provide an additional check for the experimentally determined values of compliance. Calculations were performed using the computer code FEAP [13]. The region in the immediate vicinity of the crack tip was modeled using a combination of commonly employed approaches, namely, mesh refinement and a special triangular crack-tip element [14-16]. The latter element [14,15] makes use of special interpolation functions to approximate the expected square-root dependency of the displacements on distance ahead of the crack tip. The region covered by this special element was limited to  $\sim a/1000$  (where  $a$  is the crack length) with the balance of the mesh constructed of standard 9-node quadrilaterals. Plane-strain conditions were assumed for all calculations. A typical mesh with approximately 5000 degrees of freedom is shown in Fig. 3.

### Results and Discussion

#### Back-Face Strain Compliance

The experimental compliance results are shown graphically in Fig. 4. Here, the back-face strain compliance calibration is presented as the nondimensional strain compliance function

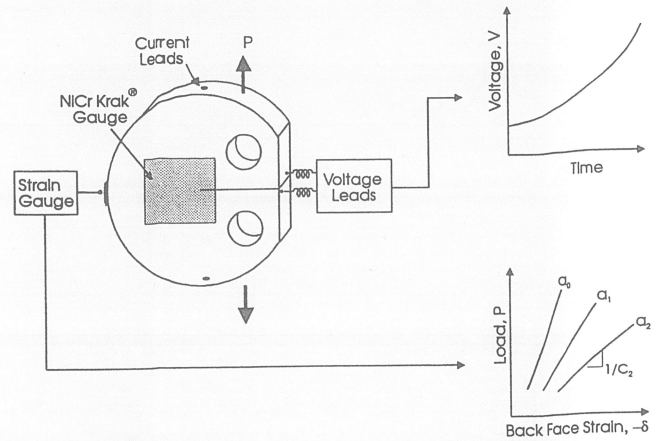


FIG. 2—Schematic illustration showing the experimental setup for both the electrical-potential crack length and back-face strain compliance calibrations.

— $EBCW$ , i.e., compliance normalized by the Young's modulus  $E$  and dimensions  $B$  and  $W$ , as a function of the crack length to width ratio  $a/W$ ; in this form, the calibration is universal for the DC(T) geometry. The corresponding polynomial calibration function, numerically fit to these data, is given in Table 1. This function describes the experimental data to better than 5%. It is considered that this calibration is good for  $a/W \leq 0.8$ , as at larger crack sizes experimental error can become significant due to the rapidly growing sensitivity of compliance to crack length and gage placement. This function has been rearranged in Table 2 to express  $a/W$  as a function of back-face strain compliance. In this form, the expression is useful for direct measurement of crack length.

The FEM results for back-face strain compliance are indicated along with the experimental data in Fig. 4. Note the good agreement with the experimentally determined calibration curve for

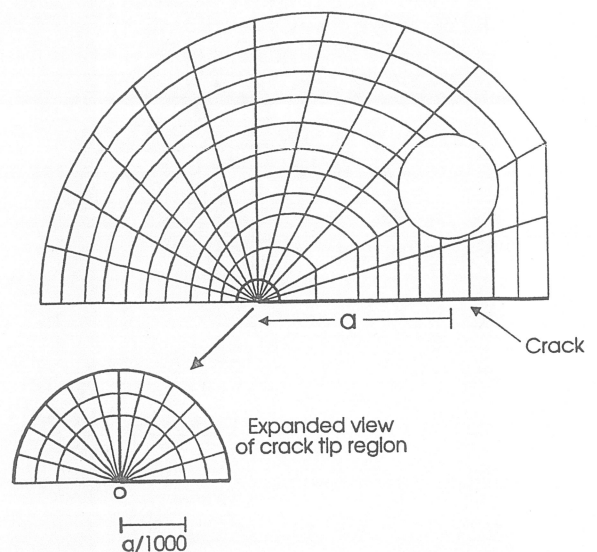


FIG. 3—Diagram illustrating a typical mesh used in the finite-element calculations. A detail of the near-tip region indicates the form of the special triangular crack-tip element [14,15], with the crack tip located at position "o." Note that the actual mesh is much finer, and has been presented in this manner for the sake of clarity.

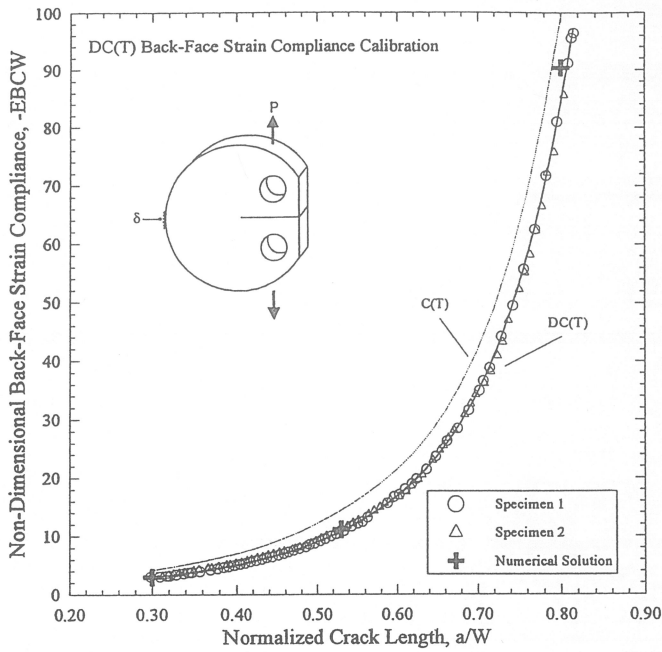


FIG. 4—A plot of the DC(T) back-face strain compliance calibration showing both the experimental data (open symbols) and the numerical solution (filled crosses), along with the polynomial fit function (solid line). The calibration for the C(T) specimen is included for comparison [5].

TABLE 1—Back-face elastic strain compliance calibration function:  $-EBCW = \alpha_0 + \alpha_1(a/W) + \alpha_2(a/W)^2 + \alpha_3(a/W)^3 + \alpha_4(a/W)^4 + \alpha_5(a/W)^5 + \alpha_6(a/W)^6$

Degree, $i$	Coefficient, $\alpha_i$
0	398.711
1	-5155.94
2	27392.4
3	-76293.7
4	118023.0
5	-96299.1
6	32629.6

TABLE 2—Inverse back-face elastic strain compliance calibration function for crack length measurement:  $a/W = \alpha'_0 + \alpha'_1 U + \alpha'_2 U^2 + \alpha'_3 U^3 + \alpha'_4 U^4 + \alpha'_5 U^5 + \alpha'_6 U^6$  where  $U = \frac{1}{\sqrt{-EBCW} + 1}$

Degree, $i$	Coefficient, $\alpha'_i$
0	0.796239
1	5.40205
2	-103.821
3	714.676
4	-2603.44
5	4829.01
6	-3578.51

$a/W = 0.3$  and  $0.53$ , where the  $-EBCW$  variation is 2.5% and 2.2%, respectively. For  $a/W = 0.8$ , however, the variation between FEM and experimentally determined  $-EBCW$  has increased to 8%, presumably due to increased sensitivity to gage placement. The FEM-determined strain variation along the back face, depicted in Fig. 5 for various values of  $a/W$ , indicates that

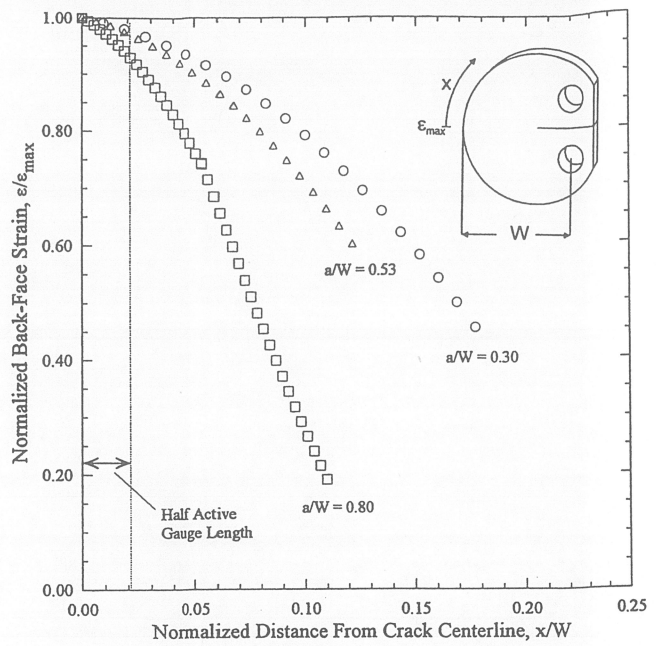


FIG. 5—Numerically obtained back-face strain gradients at three different values of  $a/W$ , plotted in terms of the normalized back-face strain,  $\epsilon/\epsilon_{max}$ , as a function of the normalized distance along the back-face,  $x/W$ , (measured from the crack centerline). The dotted line indicates the boundary of the active strain gage used in this calibration study. Note the general increase in the severity of the strain gradient as the crack approaches the back of the specimen, indicating the importance of precise gage placement for large values of  $a/W$ .

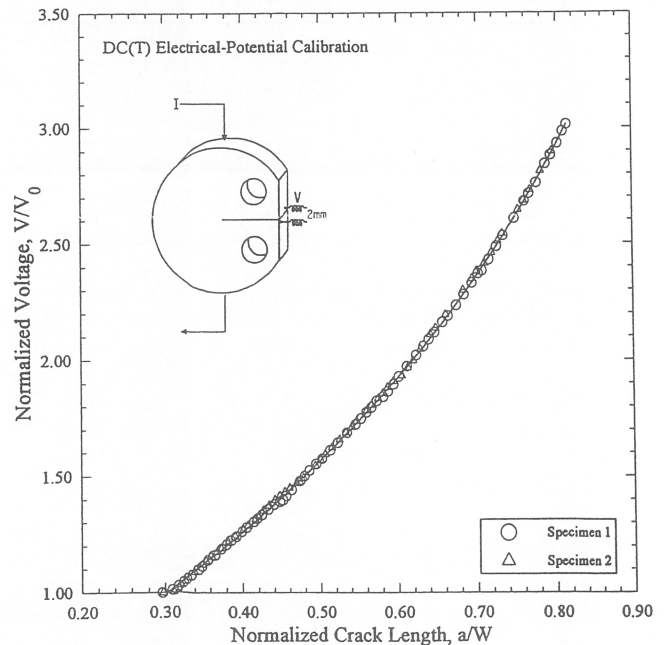


FIG. 6—The DC(T) electrical-potential crack length calibration plotted in terms of normalized voltage,  $V/V_0$ , as a function of normalized crack length,  $a/W$ , including both the experimental data (open symbols) and the polynomial fit function (solid line).

TABLE 3—Electrical-potential calibration function:  
 $V/V_0 = \beta_0 + \beta_1(a/W) + \beta_2(a/W)^2 + \beta_3(a/W)^3 + \beta_4(a/W)^4$

Degree, $i$	Coefficient, $\alpha_i$
0	0.294456
1	1.76179
2	2.88489
3	-4.95404
4	4.67002

experimental measurements should be reasonably insensitive to gage placement over most of the range of  $a/W$ . This sensitivity to placement, however, increases with crack length, and may explain the increased variation between theoretical and experimental results at the higher value of  $a/W$ .

#### Electrical-Potential Calibration

The electrical-potential calibration for crack length monitoring is shown in Fig. 6 as the potential ratio,  $V/V_0$ , as a function of  $a/W$ . Excellent agreement at all values of  $a/W$  was found between each of the two calibration specimens. Table 3 shows the corresponding polynomial calibration coefficients, describing the data to within 2%; this function is rearranged in Table 4 to express  $a/W$  in terms of  $V/V_0$  for direct crack-length measurement.

#### Summary and Conclusions

A back-face strain compliance calibration for the disk-shaped compact tension DC(T) specimen has been performed. Good agreement was obtained between numerically and experimentally determined back-face strain compliance for values of  $a/W$  less than 0.8. An increased discrepancy between experimental and numerical results was observed at large values of  $a/W$  likely due to an increasingly steep strain gradient at the back face, a condition that necessitates precise and consistent placement of the gage. This problem, however, appears negligible at smaller normalized crack lengths due to minimal strain gradients across the active gage length as determined by finite-element modeling.

In addition, an electrical-potential crack length calibration for the DC(T) geometry was experimentally determined. Excellent reproducibility was observed between each of the test specimens, and this calibration is considered usable over the range  $0.3 \leq a/W \leq 0.8$ .

TABLE 4—Inverse electrical-potential calibration function for crack length measurement:  $a/W = \beta'_0 + \beta'_1(V/V_0) + \beta'_2(V/V_0)^2 + \beta'_3(V/V_0)^3 + \beta'_4(V/V_0)^4$

Degree, $i$	Coefficient, $\alpha_i$
0	-0.0886885
1	0.380659
2	0.0531323
3	-0.0465423
4	0.00662853

#### Acknowledgments

This work was supported by the Director, Office of Energy Research, Office of Basic Energy Sciences, Materials Sciences Division of the U.S. Department of Energy under Contract DE-AC03-76SF00098. The authors would also like to thank Professors R. L. Taylor and J. C. Simo for access to the finite element code FEAP.

#### References

- [1] Ritchie, R. O. and Dauskardt, R. H., "Cyclic Fatigue of Ceramics: A Fracture Mechanics Approach to Subcritical Crack Growth and Life Prediction," *Journal of the Ceramic Society of Japan*, Vol. 99, No. 10, 1991, pp. 1047-1062.
- [2] Ritchie, R. O., Dauskardt, R. H., Yu, W., and Brendzel, A. M., "Cyclic Fatigue-Crack Propagation, Stress-Corrosion, and Fracture-Toughness Behavior in Pyrolytic Carbon-Coated Graphite for Prosthetic Heart Valve Applications," *Journal of Biomedical Materials Research*, Vol. 24, 1990, pp. 189-206.
- [3] Venkateswara Rao, K. T., Soboyejo, W. O., and Ritchie, R. O., "Ductile-Phase Toughening and Fatigue-Crack Growth in Nb-Reinforced Molybdenum Disilicide Intermetallic Composites," *Metallurgical Transactions A*, Vol. 23A, 1992, pp. 2249-2257.
- [4] Newman, J. C. Jr., "Stress Intensity Factors and Crack Opening Displacements for Round Compact Specimens," *International Journal of Fracture*, Vol. 17, No. 6, 1981, pp. 567-578.
- [5] Maxwell, D. C., "Strain Based Compliance Method for Determining Crack Length for a C(T) Specimen," *Technical Report AFWAL-TR-87-4046*, Materials Laboratory, Air Force Wright Aeronautical Laboratories, Wright-Patterson AFB, July 1987.
- [6] Ritchie, R. O. and Yu, W., "Short Crack Effects in Fatigue: A Consequence of Crack Tip Shielding," in *Small Fatigue Cracks*, R. O. Ritchie and J. Lankford, Eds., The Metallurgical Society of the American Institute of Mining, Metallurgical and Petroleum Engineers, Warrendale, PA, 1986, pp. 167-189.
- [7] Ritchie, R. O., Yu, W., and Bucci, R. J., "Fatigue Crack Propagation in ARALL Laminates: Measurement of the Effect of Crack-Tip Shielding from Crack Bridging," *Engineering Fracture Mechanics*, Vol. 32, No. 3, 1989, pp. 361-377.
- [8] Evans, A. G., "The New High-Toughness Ceramics," in *Fracture Mechanics: Perspectives and Directions (Twentieth Symposium)*, ASTM STP 1020, R. P. Wei and R. P. Gangloff, Eds., American Society for Testing and Materials, Philadelphia, 1989, pp. 267-291.
- [9] Steinbrech, R. W., "Toughening Mechanisms for Ceramic Materials," *Journal of the European Ceramic Society*, Vol. 10, 1992, pp. 131-142.
- [10] Ritchie, R. O., "Mechanisms of Fatigue Crack Propagation in Metals, Ceramics and Composites: Role of Crack Tip Shielding," *Materials Science and Engineering*, Vol. 103, 1988, pp. 15-28.
- [11] Utah, D. A., Cullen, W. H., Ritchie, R. O., et al., "Fatigue Crack Propagation," in *Metals Handbook Ninth Edition: Volume 8, Mechanical Testing*, American Society for Metals, Metals Park, OH, 1985, pp. 376-402.
- [12] Aronson, G. H. and Ritchie, R. O., "Optimization of the Electrical Potential Technique for Crack Growth Monitoring in Compact Test Pieces Using Finite Element Analysis," *Journal of Testing and Evaluation*, Vol. 7, No. 4, 1979, pp. 208-215.
- [13] Zienkiewicz, O. C. and Taylor, R. L., *The Finite Element Method*, 4th ed., Vol. 1, McGraw-Hill Book Co., London, 1989, pp. 436-583.
- [14] Stern, M. and Becker, E. B., "A Conforming Crack Tip Element with Quadratic Variation in the Singular Fields," *International Journal for Numerical Methods in Engineering*, Vol. 12, 1978, pp. 279-288.
- [15] Stern, M., "Families of Consistent Conforming Elements with Singular Derivative Fields," *International Journal for Numerical Methods in Engineering*, Vol. 14, 1979, pp. 409-421.
- [16] Chan, S. K., Tuba, I. S., and Wilson, W. K., "On the Finite Element Method in Linear Fracture Mechanics," *Engineering Fracture Mechanics*, Vol. 2, No. 1, 1970, pp. 1-17.